Nanosheet controlled epitaxial growth of PbZr0.52Ti0.48O3 thin films on glass substrates

M. Bayraktar, A. Chopra, F. Bijkerk, and G. Rijnders

Citation: Applied Physics Letters **105**, 132904 (2014); doi: 10.1063/1.4896991
View online: http://dx.doi.org/10.1063/1.4896991
View Table of Contents: http://scitation.aip.org/content/aip/journal/apl/105/13?ver=pdfcov
Published by the AIP Publishing

Nanosheet controlled epitaxial growth of $PbZr_{0.52}Ti_{0.48}O_3$ thin films on glass substrates

M. Bayraktar,[1,a)] A. Chopra,[2,a)] F. Bijkerk,[3] and G. Rijnders[2,b)]
[1]*Laser Physics and Nonlinear Optics Group, MESA+ Institute for Nanotechnology, University of Twente, P.O. Box 217, 7500 AE Enschede, The Netherlands*
[2]*Inorganic Materials Science Group, MESA+ Institute for Nanotechnology, University of Twente, P.O. Box 217, 7500 AE Enschede, The Netherlands*
[3]*Industrial Focus Group XUV Optics, MESA+ Institute for Nanotechnology, University of Twente, P.O. Box 217, 7500 AE Enschede, The Netherlands*

(Received 1 July 2014; accepted 14 September 2014; published online 1 October 2014)

Integration of $PbZr_{0.52}Ti_{0.48}O_3$ (PZT) films on glass substrates is of high importance for device applications. However, to make use of the superior ferro- and piezoelectric properties of PZT, well-oriented crystalline or epitaxial growth with control of the crystal orientation is a prerequisite. In this article, we report on epitaxial growth of PZT films with (100)- and (110)-orientation achieved by utilizing $Ca_2Nb_3O_{10}$ (CNO) and $Ti_{0.87}O_2$ (TO) nanosheets as crystalline buffer layers. Fatigue measurements demonstrated stable ferroelectric properties of these films up to 5×10^9 cycles. (100)-oriented PZT films on CNO nanosheets show a large remnant polarization of 21 $\mu C/cm^2$ that is the highest remnant polarization value compared to (110)-oriented and polycrystalline films reported in this work. A piezoelectric response of 98 pm/V is observed for (100)-oriented PZT film which is higher than the values reported in the literature on Si substrates. © *2014 AIP Publishing LLC*.
[http://dx.doi.org/10.1063/1.4896991]

In the last few decades, lead zirconate titanate, $PbZr_xTi_{1-x}O_3$ (PZT), thin films have found a plethora of applications in microelectromechanical systems (MEMS)[1] and memory devices.[2] The choice of PZT in these applications stems from its remarkable ferroelectric and piezoelectric properties.[3] These properties are strongly related to the quality of the crystal growth and the orientation of the PZT thin films,[4,5] therefore well-oriented crystalline growth or epitaxial growth with control of the orientation is highly desired. In addition, stability of the ferroelectric response after many switching cycles is a vital factor for long-term operation of the fabricated devices. $SrTiO_3$ (STO),[6,7] MgO,[8] and $LaAlO_3$ (LAO)[9] substrates facilitate the epitaxial growth of PZT films due to three factors. (a) These substrates are stable against oxidation in the substrate thin film interface, (b) they are single crystalline, and (c) the mismatch in the in-plane lattice parameters between the substrate and the film is small. On the other hand, these substrates are difficult to process and expensive, therefore they have limited use in practical device applications. For practical applications, integration of PZT films on widely used inexpensive substrates such as Si and glass is required. Integration on glass is of high importance in order to pave the way to integrate PZT on amorphous structures, such as SiO_2 that is commonly used in semiconductor devices and Mo/Si mirror coatings for extreme ultraviolet (EUV) photolithography.[10,11]

Deposition of oxide films, including PZT, directly on Si substrates results in inter-diffusion of oxides into Si and formation of amorphous oxide layer in the substrate-film interface, therefore buffer layers are utilized to prevent the inter-diffusion process. STO and yttria-stabilized zirconia (YSZ)/CeO_2 are such buffer layers that are commonly used to integrate epitaxial PZT films on Si substrates.[12–15] However, growth of these buffer layers require high temperatures; therefore, they are not suitable for many applications. Integration of PZT films on Si using Pt buffer layers (also serves as bottom electrode) is a low temperature process, but the films show poor ferroelectric properties.[16,17] Recently, integration of PZT films on Si have been achieved using nanometer-thick crystalline layers, namely nanosheets.[18] Since the integration using nanosheets was achieved at 600 °C, this gives an opportunity to extend the integration of PZT on glass using nanosheets.

Initial growth studies on glass for flat panel display applications suffer from both mixed growth (pyrochlore and perovskite phase) and random orientation of the PZT films.[19–24] It is well known that the electrode material has a large impact on the growth quality, crystalline orientation and ferroelectric properties.[14,25–28] Depositions on Pt or Au electrodes that are known to have preferential growth at low temperatures minimized the pyrochlore phase, but the resulting PZT films are polycrystalline.[29–32] Using conductive oxide electrodes such as $SrRuO_3$ (SRO) and $LaNiO_3$ (LNO), the orientation control has been improved and undesired crystal orientations have been reduced.[33–36] On the other hand, in these studies, there is no detailed investigation of the piezoelectric properties, which is vital for device applications.

In this paper, we report on the growth of epitaxial (100)-oriented and preferentially (110)-oriented PZT films with LNO electrodes on glass substrates using $Ca_2Nb_3O_{10}$ (CNO) and $Ti_{0.87}O_2$ (TO) nanosheet buffer layers, respectively. For comparison, a PZT film on Pt coated glass substrate was deposited under same growth conditions. In comparison to the PZT film deposited on Pt coated substrates, improved ferroelectric and piezoelectric properties were observed for the

[a)]M. Bayraktar and A. Chopra contributed equally to this work.
[b)]Electronic mail: a.j.h.m.rijnders@utwente.nl

PZT films deposited on nanosheet buffered substrates. The whole PZT integration process including top and bottom electrode was achieved at growth temperature of 600 °C which makes it possible to extend the PZT deposition on amorphous structures with low processing temperatures.

The processes of nanosheets synthesis and transfer to the substrates have been done as described by Nijland *et al.*[37] The CNO and TO nanosheets were obtained from layered compounds of $KCa_2Nb_3O_{10}$ and $K_{0.8}[Ti_{1.73}Li_{0.27}]O_4$, respectively. Both layered compounds were treated by nitric acid in order to exchange potassium ions in the interlayers with protons resulting in $HCa_2Nb_3O_{10}\cdot 1.5H_2O$ and $H_{1.7}Ti_{1.73}O_4\cdot H_2O$ solutions. The protonated compounds were treated by tetrabutylammonium to exfoliate the CNO and TO nanosheets. The nanosheets were transferred to the glass substrates using Langmuir-Blodgett deposition process, resulting in a dense coverage of the substrate surface. The substrates were ultra-low expansion (ULE) glass (Corning 7972) with 500 μm thickness. Prior to the deposition, the nanosheet coated substrates were annealed at 600 °C for 60 min in 0.140 millibar oxygen pressure. This step helps to burn out any surfactant and increases the adhesion to the substrate. No peeling off was observed in the adhesion tests done with the scotch tape method. For the Pt sample, the glass substrate was first coated with 5 nm thick Ti to increase the adhesion and then with 100 nm thick Pt using radio frequency sputter deposition at room temperature.

It is well known that the ferroelectric and piezoelectric properties of the PZT films vary with the composition and the $PbZr_{0.52}Ti_{0.48}O_3$ composition at the morphotropic phase boundary (MPB) is usually preferred due to its high piezoelectric response. In this article, $PbZr_{0.52}Ti_{0.48}O_3$ films were grown using pulsed laser deposition (PLD) with a KrF excimer laser at 248 nm wavelength with 20 ns pulse duration. The PZT films were sandwiched between LNO electrodes. The base pressure of the deposition chamber was kept at 5×10^{-7} mbar before increasing the temperature. The LNO and PZT layers were deposited at 600 °C and 585 °C, respectively. Crystallographic properties were determined by a Philips X'Pert MRD x-ray diffractometer (XRD) with Cu-$K\alpha$ radiation at 0.1548 nm wavelength. The cross-sectional scanning electron microscopy (SEM) images of the heterostructures were recorded using a Zeiss MERLIN HR-SEM. In order to enhance the homogeneity of the electric field, a 100 nm thick Pt film was deposited to every sample on the LNO top electrode using radio frequency sputtering at room temperature. Capacitors of 200×200 μm^2 area were patterned using photolithography and structured using standard Argon ion etching. Current-electric field (*I-E*), polarization-electric field (*P-E*) loops, and the remnant polarization (P_r) versus number of switching cycles (fatigue) were measured using an AixACCT TF Analyzer 2000 with bipolar triangular pulses at 1 kHz. The piezoelectric responses of the films were measured using a Polytec MSA-400 laser Doppler vibrometer (LDV) operating at 8 kHz.

The measured XRD patterns of the heterostructures are shown in Fig. 1. The crystallographic peaks are labeled with pseudo-cubic indexing.[38] The peaks indicate a pure perovskite phase for all three heterostructures, and no pyrochlore phase is observed. The heterostructures on CNO, TO, and Pt

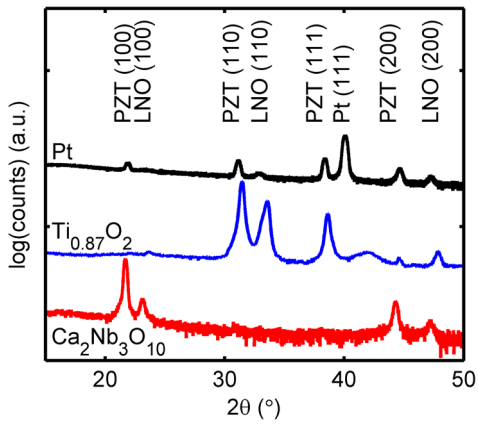

FIG. 1. XRD θ-2θ scans of the $LaNiO_3/PbZr_{0.52}Ti_{0.48}O_3/LaNiO_3$/Buffer/Glass heterostructures deposited using Pt, $Ti_{0.87}O_2$, and $Ca_2Nb_3O_{10}$ buffer layers.

yield pure (100)-oriented, preferentially (110)-oriented, and polycrystalline films, respectively. The pure (100)-oriented growth on CNO nanosheet can be attributed to the perfect match of the in-plane square lattices ($a=3.86$ Å) of the CNO and the LNO. This match prevents in-plane stress while the LNO film grows in (100) direction. Here, it is important to note that each nanosheet flake has a regular square lattice matching the lattice of the LNO film, therefore the growth is epitaxial in each flake. On the other hand, distinct flakes can be rotated with respect to each other; therefore, in-plane coherence across distinct flakes is not expected. The TO nanosheets have a 2D structure that is formed by edge linking of TiO_6 octahedra in a lepidocrocite-type rectangular 2D lattice with in-plane lattice parameters of $a=3.76$ Å and $b=2.97$ Å. The (100) face of the LNO cubic lattice ($a=3.86$ Å) has a large mismatch in *b*-parameter contrary to the close match in *a*-parameter. On the other hand, the (110) face of the LNO lattice ($a=3.86$ Å, $b=5.45$ Å) forms a close match to the two-fold lattice of the TO nanosheet ($a=3.76$ Å, $2*b=5.94$ Å). The resulting lattice mismatch, which is below 8%, is small enough to allow preferential growth in (110) direction, but it is too large to achieve pure (110) growth, as evident from the small (111) peak visible in Fig. 1. The films on Pt layer shows mixture of distinct peaks with a strong (111) Pt peak as expected.

The microstructure of the deposited films is shown in Fig. 2, as analyzed using HR-SEM. The film stacks

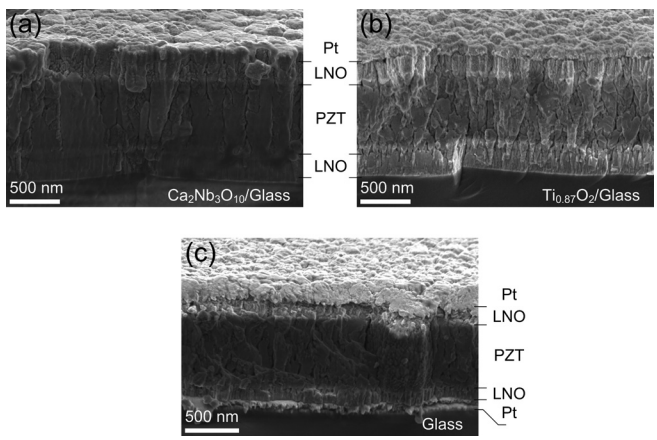

FIG. 2. SEM images of the PZT-electrode stacks with (a) $Ca_2Nb_3O_{10}$, (b) $Ti_{0.87}O_2$, and (c) Pt as buffer layers.

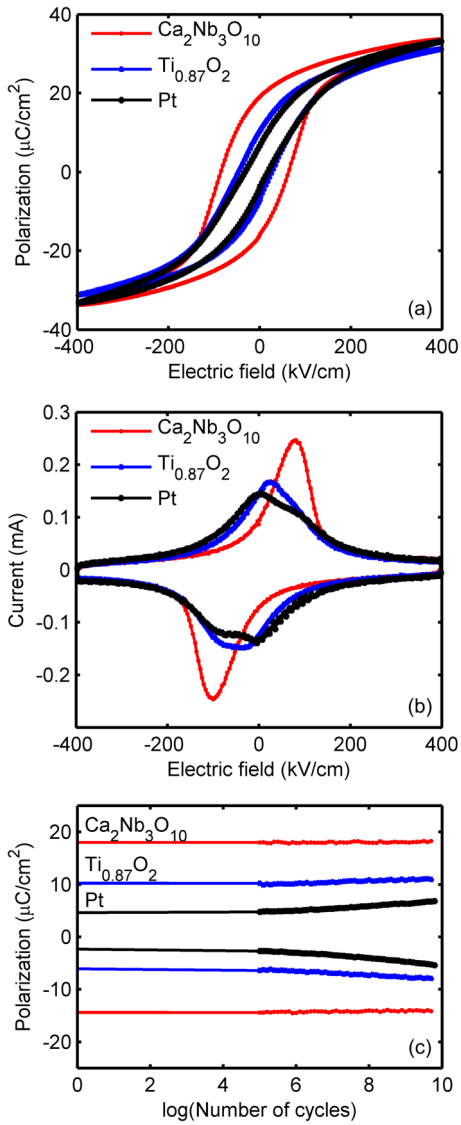

FIG. 3. (a) Polarization-electric field hysteresis loops, (b) current-electric field response, and (c) remnant polarization- versus number of switching cycles.

Pt/LNO/PZT/LNO, grown on CNO, TO and Pt layers are shown in Fig. 2(a), (b), and (c), respectively. The thicknesses of the bottom LNO, PZT, and top LNO layers are approximately 200 nm, 750 nm, and 200 nm, respectively. The LNO film on CNO nanosheets has a clearly visible interface to the PZT layer and the densest packing as compared to the TO and Pt samples.

The measured polarization-electric field hysteresis, current-electric field switching loops and remnant polarization versus number of switching cycles are shown in Figs. 3(a)–3(c), respectively. The remnant polarization (P_r) and coercive fields (E_c) of the samples derived from Fig. 3(a) are listed in Table I in comparison to the values from literature. The remnant polarization for CNO, TO, and Pt samples are 17 μC/cm^2, 8.3 μC/cm^2, and 5.1 μC/cm^2, respectively. The CNO sample has the highest and the Pt sample has the lowest remnant polarization, in relation to the epitaxial growth of the CNO sample and polycrystalline growth of the Pt sample. The remnant polarization and coercive field values from the literature show a large variation from 20 μC/cm^2 to 32 μC/cm^2 and from 33 kV/cm to 140 kV/cm, respectively. On the other hand, the remnant polarization and coercive field values for our CNO sample are comparable to the values in Ref. 34 which has the same deposition temperature.

The *I-E* switching loops plotted in Fig. 3(b) shows a much sharper current peak for CNO sample than the other two peaks indicating the higher quality of the growth. The switching loop of the Pt sample has two peaks both in positive and negative switching directions. Existence of double switching peaks is well reported in the literature and is attributed to the pinning of the domain walls.[26,39] By subsequent cycling, the domain walls are depinned leading to single switching peak. The remnant polarization of the films subjected to large number of switching cycles, namely the fatigue response, is shown in Fig. 3(c). After 5×10^9 switching cycles, the remnant polarization of the CNO and TO samples are constant as compared to the Pt sample. The remnant polarization of the Pt sample approximately doubles after the switching cycles are applied as a result of the depinning of the domain walls.

In the last step, the longitudinal piezoelectric responses ($d_{33,f}$) of the PZT films were locally measured using LDV. The samples were fixed to large metal plates with silver paste to minimize the bending of the substrate (which would affect the measurement). Maximum piezoelectric response for CNO, TO, and Pt are 98 pm/V, 49 pm/V, and 12 pm/V, respectively (Fig. 4). The difference in the piezoelectric responses is a consequence of the difference in the orientations and the growth quality. Theoretically, highest piezoelectric response is predicted to be in (100)-oriented films and lowest in (111)-

TABLE I. Ferroelectric and piezoelectric properties of the PZT films.

Materials	Temperature (°C)	Remnant polarization, P_r (μC/cm^2)	Coercive field, E_c (kV/cm)	Effective piezoelectric coefficient, $d_{33,f}$ (pm/V)	Reference
Pt/LNO/PZT/LNO/CNO/Glass	600	17	74	98	This work
Pt/LNO/PZT/LNO/TO/Glass	600	8.3	36	49	This work
Pt/LNO/PZT/LNO/Pt/Glass	600	5.1	25	12	This work
PZT/Au/Pt/NiCr/Glass	400	20	100	30	29
PZT/Pt/Ti/Glass	550	28–30	51–54	…	30
PZT/Pt/Ti/Glass	550	26	33	…	32
ITO/LNO/PZT/LNO/ITO/Glass[a]	650	29	…	…	33
Au/PZT/LNO/Glass	600	22	58	…	34
PZT/LNO/CNO/Glass	700	~30	~80	…	35
PZT/SRO/YSZ/Glass	700	32	~140	…	36

[a]ITO: In_2O_3 90% and SnO_2 10%.

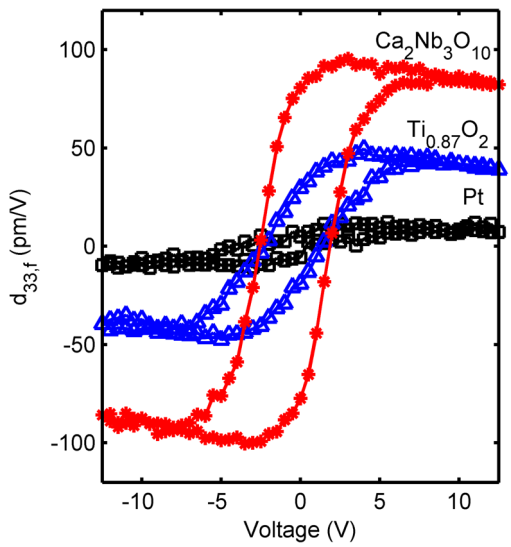

FIG. 4. Longitudinal piezoelectric response ($d_{33,f}$) of the three heterostructures measured using a laser Doppler vibrometer.

oriented films in accordance with our measurements.[5] The effective piezoelectric response depends not only on the orientation of the films but also on the ratio of the electrode size to the substrate thickness.[40,41] The CNO sample has higher piezoelectric response than the PZT films on Si substrates for similar electrode size to substrate thickness ratios.[41] Achieving this remarkable piezoelectric response on an amorphous substrate shows the effectiveness of the presented nanosheet approach in integrating ferroelectric PZT films on glass substrates.

In conclusion, we have grown and characterized epitaxial (100)-oriented and preferentially (110)-oriented $PbZr_{0.52}Ti_{0.48}O_3$ films on glass substrates using CNO and TO nanosheets. The fabricated films show comparable or higher ferroelectric and piezoelectric responses than the values reported in the literature. The presented approach can also be used in integrating PZT films on amorphous surfaces for semiconductor circuits, glass waveguides and amorphous coatings like EUV mirrors.

This research program was funded by "Stichting Technologie en Wetenschap (STW)" under the Contract 10448 with the project name "Smart Multilayer Interactive Optics for Lithography at Extreme UV wavelengths (SMILE)." The SMILE project is being sponsored by Carl Zeiss SMT GmbH. F. Bijkerk acknowledges the contributions from the FOM-Zeiss-ASML Industrial Partnership Programme CP3E. The authors would like to thank Professor J. E. ten Elshof and Mr. Maarten Nijland for providing the nanosheets and Dr. Minh Nguyen for Pt coating.

[1]S. Trolier-McKinstry and P. Muralt, J. Electroceram. **12**, 7 (2004).
[2]*Ferroelectric Thin Films*, edited by M. Okuyama and Y. Ishibashi (Springer-Verlag, Berlin Heidelberg, 2005).
[3]B. Jaffe, W. R. Cook, and H. Jaffe, *Piezoelectric Ceramics* (Academic, London, 1971).
[4]X. Du, U. Belegundu, and K. Uchino, Jpn. J. Appl. Phys., Part 1 **36**, 5580 (1997).
[5]X. Du, J. Zheng, U. Belegundu, and K. Uchino, Appl. Phys. Lett. **72**, 2421 (1998).
[6]L. X. Cao, Y. Xu, B. R. Zhao, L. P. Guo, L. Li, B. Xu, Y. Z. Zhang, H. Chen, A. J. Zhu, Z. H. Mai, J. H. Zhao, Y. F. Fu, and X. J. Li, J. Phys. D: Appl. Phys. **30**, 1455 (1997).
[7]I. Vrejoiu, G. Le. Rhun, L. Pintilie, D. Hesse, M. Alexe, and U. Gösele, Adv. Mater. **18**, 1657 (2006).
[8]G. Barucca, A. De. Benedittis, A. Di. Cristoforo, G. Majni, P. Mengucci, F. Leccabue, and B. E. Watts, Thin Solid Films **319**, 207 (1998).
[9]J. H. Kim and F. F. Lange, J. Mater. Res. **14**, 4004 (1999).
[10]M. Bayraktar, W. A. Wessels, C. J. Lee, F. A. van Goor, G. Koster, G. Rijnders, and F. Bijkerk, J. Phys. D: Appl. Phys. **45**, 494001 (2012).
[11]E. Louis, A. E. Yakshin, T. Tsarfati, and F. Bijkerk, Prog. Surf. Sci. **86**, 255 (2011).
[12]D. K. Fork, D. B. Fenner, G. A. N. Connell, J. M. Phillips, and T. H. Geballe, Appl. Phys. Lett. **57**, 1137 (1990).
[13]S. J. Wang, C. K. Ong, L. P. You, and S. Y. Xu, Semicond. Sci. Technol. **15**, 836 (2000).
[14]M. Dekkers, M. D. Nguyen, R. Steenwelle, P. M. te Riele, D. H. A. Blank, and G. Rijnders, Appl. Phys. Lett. **95**, 012902 (2009).
[15]A. Chopra, D. Pantel, Y. Kim, M. Alexe, and D. Hesse, J. Appl. Phys. **114**, 084107 (2013).
[16]J. G. E. Gardeniers, A. Smith, and C. Cobianu, J. Micromech. Microeng. **5**, 153 (1995).
[17]A. Kumar, M. R. Alam, A. Mangiaracina, and M. Shamsuzzoha, J. Electron. Mater. **26**, 1331 (1997).
[18]Y. Minemura, K. Nagasaka, T. Kiguchi, T. J. Konno, H. Funakubo, and H. Uchida, Jpn. J. Appl. Phys., Part 1 **52**, 09KA04 (2013).
[19]X. M. Lu, J. S. Zhu, X. F. Huang, C. Y. Lin, and Y. N. Wang, Appl. Phys. Lett. **65**, 2015 (1994).
[20]X. M. Lu, J. S. Zhu, W. S. Hu, Z. G. Liu, and Y. N. Wang, Appl. Phys. Lett. **66**, 2481 (1995).
[21]S.-I. Kuroki, K. Tago, K. Kotani, and T. Ito, Jpn. J. Appl. Phys., Part 1 **48**, 04C142 (2009).
[22]J. Jiang, S.-I. Kuroki, K. Kotani, and T. Ito, Jpn. J. Appl. Phys., Part 1 **49**, 04DH14 (2010).
[23]S. S. Roy, H. Gleeson, C. P. Shaw, R. W. Whatmore, Z. Huang, Q. Zhang, and S. Dunn, Integr. Ferroelectr. **29**, 189 (2000).
[24]E. Bruno, F. Ciuchi, M. Castriota, S. Marino, G. Nicastro, E. Cazzanelli, and N. Scaramuzza, Ferroelectrics **396**, 49 (2010).
[25]C. B. Eom, R. B. Van Dover, J. M. Phillips, D. J. Werder, J. H. Marshall, C. H. Chen, R. J. Cava, R. M. Fleming, and D. K. Fork, Appl. Phys. Lett. **63**, 2570 (1993).
[26]M.-S. Chen, T.-B. Wu, and J.-M. Wu, Appl. Phys. Lett. **68**, 1430 (1996).
[27]J. Lee, C. H. Choi, B. H. Park, T. W. Noh, and J. K. Lee, Appl. Phys. Lett. **72**, 3380 (1998).
[28]C. W. Law, K. Y. Tong, J. H. Li, K. Li, and M. C. Poon, Thin Solid Films **354**, 162 (1999).
[29]P. Verardi, M. Dinescu, F. Craciun, R. Dinu, and M. F. Ciobanu, Appl. Phys. A **69**(Suppl.), S837 (1999).
[30]R. H. T. Wilke, S. Trolier-McKinstry, P. B. Reid, and D. A. Schwartz, Proc. SPIE **7803**, 78030O (2010).
[31]D. H. Kim, Y. K. Kim, S. Hong, Y. Kim, and S. Baik, Nanotechnology **22**, 245705 (2011).
[32]R. H. T. Wilke, R. L. Johnson-Wilke, V. Cotroneo, W. N. Davis, P. B. Reid, D. A. Schwartz, and S. Trolier-McKinstry, App. Opt. **52**, 3412 (2013).
[33]K. K. Uprety, L. E. Ocola, and O. Auciello, J. Appl. Phys. **102**, 084107 (2007).
[34]Y. H. Yu, M. O. Lai, and L. Lu, Appl. Phys. A **88**, 365 (2007).
[35]K. Kikuta, K. Noda, S. Okumura, T. Yamaguchi, and S. Hirano, J. Sol-Gel Sci. Technol. **42**, 381 (2007).
[36]J. Y. Son and Y.-H. Shin, Electrochem. Solid-State Lett. **12**, G20 (2009).
[37]M. Nijland, S. Kumar, R. Lubbers, D. H. A. Blank, G. Rijnders, G. Koster, and J. E. ten Elshof, ACS Appl. Mater. Interfaces **6**, 2777 (2014).
[38]JCPDS card numbers are Pt: 87-0647, $LaNiO_3$: 33-0710, and $PbZr_{0.52}Ti_{0.48}O_3$: 56-0900.
[39]T. Rojac, M. Kosec, B. Budic, N. Setter, and D. Damjanovic, J. Appl. Phys. **108**, 074107 (2010).
[40]P. Gerber, A. Roelofs, C. Kügeler, U. Böttger, R. Waser, and K. Prume, J. Appl. Phys. **96**, 2800 (2004).
[41]S. Sivaramakrishnan, P. Mardilovich, A. Mason, A. Roelofs, T. Schmitz-Kempen, and S. Tiedke, Appl. Phys. Lett. **103**, 132904 (2013).